Polyphase-Coded FM (PCFM) Radar Waveforms, Part II: Optimization

[1]Shannon D. Blunt, *IEEE Senior Member,* [1]John Jakabosky, *IEEE Student Member,* [2]Matthew Cook, *IEEE Member,* [1]James Stiles, *IEEE Senior Member,* [1]Sarah Seguin, *IEEE Member*, and [3]Eric L. Mokole, *IEEE Fellow*

[1]S.D. Blunt, J. Jakabosky, J. Stiles, and S. Seguin are with the Electrical Engineering & Computer Science Dept., Radar Systems & Remote Sensing Lab, of the University of Kansas, Lawrence, KS.

[2]M. Cook is with the University of Kansas and Garmin International in Olathe, KS.

[3]E.L. Mokole is with the Radar Division of the US Naval Research Laboratory, Washington, DC.

Abstract

This paper addresses polyphase code optimization with respect to the nonlinear FM waveform generated by the CPM implementation. A greedy search leveraging the complementary metrics of PSL, ISL, and spectral content yield extremely low range sidelobes relative to waveform time-bandwidth product. Transmitter distortion is also incorporated into the optimization via modeling and actual hardware. Thus the physical radar emission can be designed to address spectrum management and enable the physical realization of advanced waveform-diverse schemes.

Keywords

I. INTRODUCTION

The traditional approach to nonlinear FM (NLFM) waveform design relies on the identification of a suitable continuous phase/frequency function of time (see Sect. 5.2 of [3] for an overview). Many such methods are based on the principle of stationary phase [4–6], which relates the power spectral density and the chirp rate at each frequency and thereby shapes the spectral content of the waveform accordingly. Another class of NLFM is hyperbolic FM (HFM), otherwise known as linear period modulation (LPM) [7,8]. Other design approaches include higher-order polynomials [9], use of the Zak transform [10], and hybrid methods that also employ amplitude tapering on receive [11,12]. In this paper, the authors explore the optimization of the class of NLFM waveforms denoted as polyphase-coded FM (PCFM) that are made possible through the continuous phase modulation (CPM) implementation.

In the companion paper [13], it was shown that the CPM implementation commonly used for aeronautical telemetry, deep-space communications, and Bluetooth devices can

be modified to implement arbitrary polyphase radar codes as PCFM waveforms. With the use of appropriate mismatch filtering on receive to compensate for increased range sidelobes resulting from *design mismatch*, this scheme provides a means to use the large existing library of polyphase codes on high-power radar systems. Furthermore, this new code/waveform linkage provides the opportunity to optimize a code according to the characteristics of the resulting continuous waveform, thereby ameliorating the design mismatch problem. Such an approach can likewise be extended to incorporate the distortion induced by the physical transmitter and thus facilitate actual physical *emission optimization*.

The virtue of a coded structure is that its discrete nature allows for optimization of the temporal signature through various code-search strategies [14–16]. Extension of this discrete structure into the continuous domain via appropriate implementation [13] and through the subsequent transmitter distortion thus provides a framework for optimizing physical emissions by these same code-search strategies. Figure 1 illustrates this general notion of emission optimization in which a candidate polyphase code is selected, is implemented as a continuous PCFM waveform via CPM, and then is injected into the transmitter where the waveform encounters spectral shaping and nonlinear effects. Assessment of the resulting physical emission (a distorted version of the waveform) is used to close the optimization loop and thereby drive the code-search process.
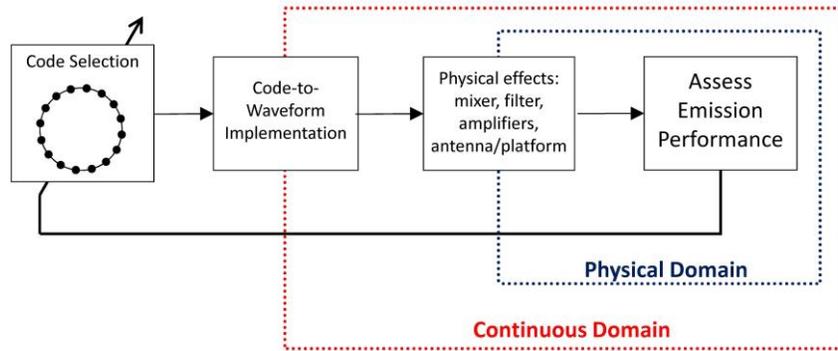
Figure 1: Notional representation of the optimization of physical radar emissions

Cast in the manner of Fig. 1 using the CPM implementation, the emission optimization problem involves the determination of a sequence of N phase values (more specifically, phase *change* values). If each of these N values can take on one of L possible states, then there exist L^N possible coded emissions (assuming, for operational time scales, that the transmitter behavior is time invariant). For even modest values of N and L, the computational requirements to search all possibilities quickly become intractable, thus necessitating the search for adequate suboptimal solutions. Consequently, a variation of the greedy code-search strategy known as Marginal Fisher's Information (MFI) [16], recently demonstrated as an effective means to search a high-dimensional solution space, is employed. While the high dimensionality precludes the practical determination of a globally optimal solution, it is shown that this greedy approach yields effective suboptimal results, in part by leveraging a "performance diversity" concept that alternates among multiple different, yet complementary, performance metrics. Also, for some sensing applications, the argument can be made that many "good enough" emissions are even preferable to a single "best" emission.

For emission optimization, three operational paradigms are considered: 1) an idealized distortion-free transmitter; 2) transmitter distortion defined by a mathematical

model; and 3) incorporation of a physical transmitter. The distortion-free case is included to demonstrate the potential of optimizing PCFM waveforms in this manner, with the special classes of linear FM (LFM) [3, Sect. 4.2] and hyperbolic FM (HFM) [7,8] waveforms used as benchmarks for comparison. Using mathematical models for transmitter distortion [17] provides an efficient way to account for realistic transmitter effects. This Model-in-the-Loop (MiLo) version of emission optimization may be useful to determine the potential capabilities and deficiencies of various transmitter components/topologies and may also serve as a starting point for inclusion of the physical transmitter in the optimization process. Note that the efficacy of the MiLo approach is clearly dependent upon how well the mathematical model reflects reality. Finally, Hardware-in-the-Loop (HiLo) emission design involves the incorporation of a physical transmitter into the optimization procedure. An L-band radar test bed at the University of Kansas is used to demonstrate HiLo design.

The remainder of the paper is organized as follows. Section II establishes a formal framework that connects the discrete code to the physical emission, thus facilitating optimization. Section III discusses the code-search process used herein and the various optimization criteria. In Section IV, the distortion-free case is considered, and optimized PCFM waveforms are assessed according to standard benchmarks. Finally, the capability to optimize physical emissions for MiLo and HiLo schemes is demonstrated (Section V).

II. CODIFYING THE EMISSION

As shown in Figure 1, the physical PCFM radar emission can be characterized by three stages: 1) an underlying discrete code comprised of a sequence of phase values that

2) undergoes a transformation into a continuous signal followed by 3) a subsequent transformation representing the distortion imparted by the transmitter. Per the formulation in [13], let θ_0, θ_1, θ_2, $\cdots$, θ_N represent the collection of $N+1$ phase values in a constant-envelope polyphase code. The set α_1, α_2, $\cdots$, α_N is thus the collection of "shortest path" phase changes between the pairs of adjacent phase values (see (1) and (2) in [13]). Noting that the initial phase θ_0 is arbitrary with regard to the set of N phase changes, the structure of the code can be compactly represented as the length-N vector

$$\mathbf{x} = \begin{bmatrix} \alpha_1 & \alpha_2 & \cdots & \alpha_N \end{bmatrix}^T. \tag{1}$$

The continuous phase modulation (CPM) implementation of radar codes can be expressed in a compact manner as the composite operator

$$s(t;\mathbf{x}) = T_{\text{CPM}}\{\mathbf{x}\} \tag{2}$$

representing [13, Fig. 4] that generates the continuous-time PCFM waveform associated with the particular phase-change code $\mathbf{x}$. Likewise, the distortion imparted by the transmitter onto the continuous waveform can be represented by the operation

$$u(t;\mathbf{x}) = T_{\text{Tx}}\big[s(t;\mathbf{x})\big] = T_{\text{Tx}}\Big[T_{\text{CPM}}\{\mathbf{x}\}\Big] , \tag{3}$$

which produces the physical emission launched from the radar. Finally, defining the operation $\Phi\big[u(t;\mathbf{x})\big]$ as the performance evaluation of the resulting emission according to some desired characteristic(s) like peak sidelobe level (PSL), integrated sidelobe level (ISL), spectral containment, etc., the design problem can thus be stated as:

"optimize $\Phi\big[u(t;\mathbf{x})\big]$ by selecting the parameters in $\mathbf{x} = \begin{bmatrix} \alpha_1 & \alpha_2 & \cdots & \alpha_N \end{bmatrix}^T$"

according to a specified criteria for Φ (see Section III.D). Hence, the notional emission generation and optimization framework of Fig. 1 can be illustrated from a mathematical perspective as shown in Fig. 2.
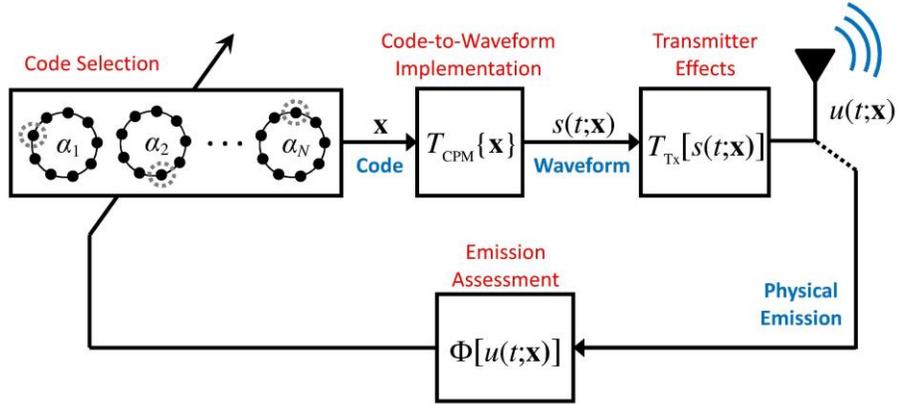

Figure 2: **Mathematical representation for the optimization of PCFM radar emissions**

While it is beyond the scope of this present work to explore it in depth, the specific nature of the transmission operator T_{Tx} plays an important role in the actual radar emission. Here, as a proof of concept, a standard transmitter distortion model and a specific hardware instantiation are considered. However, the myriad combinations of transmitter components and design topologies [18], combined with physical effects such as mutual coupling and calibration of antenna arrays [19–21], as well as emerging operating modalities such as MIMO [22] and adaptive waveform design [15], all serve to illustrate a rich research problem with regard to the modeling, design, and incorporation of the effect of T_{Tx}. It is clear that significant advances will necessarily require a holistic consideration of the signal processing (waveform generation and receive processing), the systems engineering attributes/capabilities for the particular sensing modality, and the physical electromagnetic (EM) effects at the given operating frequencies. Also note that, for a physical system, there is a practical limit to how well the modeled T_{Tx} can actually be known, thus promoting the concerted use of both MiLo and HiLo approaches.

III. SEARCHING FOR OPTIMALITY

Numerous approaches exist for searching the L^N possible coded emissions (genetic algorithms, simulated annealing, etc.) with varying degrees of speed and effectiveness. In contrast to a traditional code-search effort, the computational burden of the present problem is more onerous due to the generation of the physical emission via (2) and (3) and the subsequent evaluation of $\Phi[u(t;\mathbf{x})]$. The following subsections outline the general search strategy used herein, as well as some specific procedures to enhance and accelerate the search. A multi-metric performance framework is also incorporated that aids in the avoidance of inadequate locally optimal solutions.

A) Systematic Search for Optimized Emissions

The search strategy used here is a piecewise greedy approach whereby $N-1$ parameters in the phase-change vector $\mathbf{x}$ are held constant while the remaining parameter is perturbed to each of the L possible phase-change values [16]. The particular perturbed value (say the ℓth) of this n^{th} parameter that provides the greatest improvement according to the performance evaluation Φ subsequently replaces the previous value for the nth parameter, following which the process is repeated for a different parameter. If no improvement is possible, the parameter value is unchanged.

The phase change parameter α_n was defined in [13] as

$$\alpha_n \;=\; \Psi(\tilde{\alpha}_n) \;=\; \begin{cases} \tilde{\alpha}_n & \text{if } |\tilde{\alpha}_n| \le \pi \\ \tilde{\alpha}_n - 2\pi\,\text{sgn}(\tilde{\alpha}_n) & \text{if } |\tilde{\alpha}_n| > \pi \end{cases}, \tag{4}$$

where

$$\tilde{\alpha}_n = \theta_n - \theta_{n-1} \quad \text{for} \quad n = 1, \cdots, N, \tag{5}$$

sgn($\bullet$) is the signum operation, and θ_n is the phase value of the nth chip in the length-(N+1) polyphase code. Because the search process involves a piecewise perturbation of the code parameters, it is instructive to note that a search in θ space is different from a search in α space. For implementation convenience, the latter is considered.

To initialize the search process, an initial phase-change code is defined as

$$\mathbf{x}^{(0)} = \left[\alpha_1^{(0)} \ \alpha_2^{(0)} \ \cdots \ \alpha_N^{(0)} \right]^T, \tag{6}$$

which produces the continuous waveform $s(t;\mathbf{x}^{(0)}) = T_{\text{CPM}}\{\mathbf{x}^{(0)}\}$ and the subsequent physical emission $u(t;\mathbf{x}^{(0)}) = T_{\text{Tx}}\left[s(t;\mathbf{x}^{(0)}) \right] = T_{\text{Tx}}\left[T_{\text{CPM}}\{\mathbf{x}^{(0)}\} \right]$. Likewise, after the ith perturbation stage, the phase-change code is

$$\mathbf{x}^{(i)} = \left[\alpha_1^{(i)} \ \alpha_2^{(i)} \ \cdots \ \alpha_N^{(i)} \right]^T, \tag{7}$$

with associated waveform $s(t;\mathbf{x}^{(i)}) = T_{\text{CPM}}\{\mathbf{x}^{(i)}\}$ and physical emission $u(t;\mathbf{x}^{(i)}) = T_{\text{Tx}}\left[T_{\text{CPM}}\{\mathbf{x}^{(i)}\} \right]$.

If the $(i+1)^{\text{th}}$ stage involves the perturbation of the nth phase-change parameter α_n, then (7) is modified by using (4) as

$$\mathbf{x}_n^{(i+1)} = \left[\alpha_1^{(i)}, \ \cdots, \ \alpha_{n-1}^{(i)}, \ \Psi\left(\alpha_n^{(i)} + \Delta_{n,\ell} \right), \ \alpha_{n+1}^{(i)}, \ \cdots, \ \alpha_N^{(i)} \right]^T \tag{8}$$

for the L possible values of the perturbation $\Delta_{n,\ell}$, which are equally spaced on $\left[-\pi, \ \pi \right]$ including 0 (no change). With the subsequent candidate emission resulting from (8) as a function of $\Delta_{n,\ell}$ defined as

$$u(t;\mathbf{x}_n^{(i+1)}) = T_{\text{Tx}}\left[T_{\text{CPM}}\{\mathbf{x}_n^{(i+1)}\} \right], \tag{9}$$

the optimal $\Delta_{n,\hat{\ell}}$ with index $\hat{\ell}$ is thus determined by

$$\hat{\ell} = \arg \min_{\ell} \left(\Phi \left[u(t; \mathbf{x}_n^{(i+1)}) \right] - \Phi \left[u(t; \mathbf{x}^{(i)}) \right] \right) \tag{10}$$

depending on the prescribed performance metric Φ. Once the optimal perturbation value $\Delta_{n,\hat{\ell}}$ is determined, then the associated $\hat{\mathbf{x}}_n^{(i+1)}$ becomes $\mathbf{x}^{(i+1)}$. The process is then repeated for one of the other N phase-change parameters to obtain $\mathbf{x}^{(i+2)}$ and so on until the desired performance is attained for the physical emission.

B) Optimized Perturbation Ordering

In the search procedure just described, the ordering of perturbation of the phase-change parameters was not considered. From the perspective of a greedy search paradigm, it is appropriate to follow an ordering whereby the particular parameter being perturbed is the one that yields the greatest performance improvement. However, since it is not known *a priori* which parameter α_n can be perturbed to provide the greatest improvement, it is necessary to consider the perturbation of each of the N parameters separately and thereafter perform an *a posteriori* selection. Note that for the perturbation of α_n for each $n = 1, 2, \cdots, N$, the other $N-1$ parameters are held constant such that this procedure involves N separate parallel searches for the ith perturbation stage. This search process can be stated formally by extending (10) as

$$\{\hat{n}, \hat{\ell}\} = \arg \min_{n} \min_{\ell} \left(\Phi \left[u(t; \mathbf{x}_n^{(i+1)}) \right] - \Phi \left[u(t; \mathbf{x}^{(i)}) \right] \right) \tag{11}$$

such that replacing the particular $\alpha_{\hat{n}}^{(i)}$ with $\Psi \left(\alpha_{\hat{n}}^{(i)} + \Delta_{\hat{n},\hat{\ell}} \right)$ yields the most improvement in the given metric Φ.

The "super-greedy" search in (11) involves an *N*-fold increase in computational cost as compared to a pre-determined or random ordering of parameter perturbations. While parallel processing could clearly be employed to compensate for this high computational burden, a line search technique is presented to reduce the number of necessary performance evaluations.

C) Line Search in Phase Space

As stated in Section III.A, the search process necessitates the completion of a performance evaluation of each candidate emission as $\Phi\left[u(t;\mathbf{x}_n^{(i+1)})\right]$ for a discrete set of perturbation values $\Delta_{n,\ell}$ for $\ell=1,\,2,\,\cdots,L$ and a given index n. To avoid the brute force approach of evaluating the emission for all *L* values of $\Delta_{n,\ell}$ on $\left[-\pi,\pi\right]$, the well-known Fibonacci line search [23], or some variation thereof, can be used to focus successively onto the region(s) of $\Delta_{n,\ell}$ for which the greatest improvement is obtained via (10).

It is assumed that $\Phi\left[u(t;\mathbf{x}_n^{(i+1)})\right]$ is a continuous function of $\Delta_{n,\ell}$ on $\left[-\pi,\pi\right]$ for a fixed *n*, though not necessarily convex. Hence, a coarse gridding of the interval $\left[-\pi,\pi\right]$ into *J* sections can be established so that a separate line search is performed on each section, followed by a selection of the best result from among the *J* sections. The benefit of such a search strategy is evidenced by noting the impact of doubling the number of discrete phase-space values for $\Delta_{n,\ell}$ to $2L$. In this case, the brute force approach requires *L* additional performance evaluations, while the piecewise line search need only require *J* additional evaluations, which can be a significant computational savings for

modest values of *J*. For example, the results in Section IV indicate that the piecewise line search works well for $J = 4$.

D) Emission Assessment

There are multiple assessment metrics for Φ with which one could optimize emission performance. Perhaps the most common metric is the peak sidelobe level (PSL) [24], denoted Φ_{PSL}, and given by

$$\Phi_{\mathrm{PSL}}\left[\chi(\tau,\omega)\right] = \max_{\tau}\left|\frac{\chi(\tau,0)}{\chi(0,0)}\right| \quad \text{for} \quad \tau \in \left[\tau_{\mathrm{m}},T\right] , \tag{12}$$

where

$$\chi(\tau,\omega) = \int_{t=-T}^{+T} e^{j\omega t} u(t;\mathbf{x})\, u^{*}(t+\tau;\mathbf{x})\, dt \tag{13}$$

is the ambiguity function in terms of delay τ and Doppler frequency ω. The PSL metric in (12) considers the zero-Doppler cut of (13), where the interval $\left[-\tau_{\mathrm{m}},+\tau_{\mathrm{m}}\right]$ corresponds to the time (range) mainlobe and $\left[-T,+T\right]$ is the time support of $\chi(\tau,0)$ due to finite pulse length. The PSL metric indicates the largest degree of interference that one point scatterer can cause to another at a different range offset.

Another important metric is Φ_{ISL}, the integrated sidelobe level (ISL) [24], which for the zero-Doppler cut of the ambiguity function can be defined as

$$\Phi_{\mathrm{ISL}}\left[\chi(\tau,\omega)\right] = \frac{\displaystyle\int_{\tau_{\mathrm{m}}}^{T}\left|\chi(\tau,0)\right|d\tau}{\displaystyle\int_{0}^{\tau_{\mathrm{m}}}\left|\chi(\tau,0)\right|d\tau} . \tag{14}$$

The ISL metric is particularly useful for establishing the susceptibility to distributed scattering such as clutter.

The metrics in (12) and (14) may also be expanded to encompass non-zero Doppler by generalizing the mainlobe and sidelobe regions to correspond to the interior and exterior, respectively, of a range-Doppler ellipse. From a practical standpoint, the range-Doppler sidelobe region need only comprise a Doppler interval that depends on feasible target velocities. Thus a Doppler-tolerant aspect may also be incorporated into these metrics by defining a skewed range-Doppler mainlobe ellipse.

For code optimization approaches in the literature, PSL tends to be the most common basis for design. In contrast, most techniques to design continuous NLFM waveforms rely upon shaping of the waveform power spectral density [11] to mimic the effects of amplitude tapering while maintaining the constraint of a constant envelope. In that same vein, a spectrum-based metric that is posed in terms of the error with respect to a frequency template is defined to assess such waveforms. To that end, let $W(f)$ be a frequency weighting template (for example, a Gaussian window) that is scaled to have energy commensurate to that of a constant modulus pulse of duration T. For the emission frequency response $U(f;\mathbf{x})$, parameterized on the phase-change code $\mathbf{x}$, a frequency template error (FTE) metric Φ_{FTE} can be defined as

$$\Phi_{\mathrm{FTE}}\big[U(f;\mathbf{x})\big] = \left(\frac{1}{f_{\mathrm{H}} - f_{\mathrm{L}}}\right)\int_{f_{\mathrm{L}}}^{f_{\mathrm{H}}} \Big| \, |U(f;\mathbf{x})|^{p} - |W(f)|^{p} \, \Big|^{q} \, df \,, \qquad (15)$$

where f_{L} and f_{H} demarcate the edges of the frequency interval of interest. The values p and q define the degree of emphasis placed on different frequencies. For $p = 1$ and $q = 2$, the metric in (15) defines a form of frequency-domain mean-square error (MSE). It is this

version that shall be applied later in the paper. Alternatively, $p > 1$ overly emphasizes frequencies with higher power (in-band) and $p < 1$ overly emphasizes frequencies with lower power (out-of-band). Since the desire is to vary the phase as a free parameter for optimization, it is only the spectral envelope that is used in (15) for optimization. Also, because the power spectral density (PSD) is the Fourier transform of the autocorrelation, the PSD-based metric of (15) is complementary to metrics based on the ambiguity function (13) such as PSL (12) and ISL (14) in terms of optimizing the matched filter response of a waveform.

E) Performance Diversity

The metrics in the previous section provide different ways to assess the same fundamental goal – minimizing the range (and perhaps also Doppler) sidelobes. From an optimization perspective, these complementary metrics may be exploited to facilitate a form of *performance diversity* since each metric realizes a different performance surface with regard to the emission, especially with regard to the locations of local minima. In other words, if one metric gets stuck in a local minimum, switching to a different yet complementary metric may allow continued progress, with no further improvement occurring only in the unlikely event that all metrics experience the same local minimum. Note that while multi-objective optimization generally involves the balancing of different conflicting metrics, the multi-metric approach described here involves complementary metrics that provide different perspectives on the same criterion: lower range sidelobes.

With regard to waveform optimization consider the example of a phase transition code $\mathbf{x}$ comprised of 64 $(= N)$ elements. Figure 3 depicts the possible change in performance metric (the difference portion of (10)) when a single element of $\mathbf{x}$

(specifically, index $n = 23$) is varied over the interval $[-\pi, \pi]$ under the condition of an ideal transmitter. Note that the three (ISL, PSL, FTE) minima occur at slightly different phase transition values due to different underlying performance surfaces which, compounded over multiple optimization stages, can subsequently produce quite different waveforms at convergence. Furthermore, upon expanding to consider the best perturbation index $\hat{n}$ over the set of all 64 possible phase transitions via (11), Fig. 4 reveals that the three metrics lead to three quite different results: the PSL metric indicates $\hat{n} = 51$ is the best phase transition to perturb; while ISL and FTE metrics indicate $\hat{n} = 59$ and $\hat{n} = 61$, respectively.
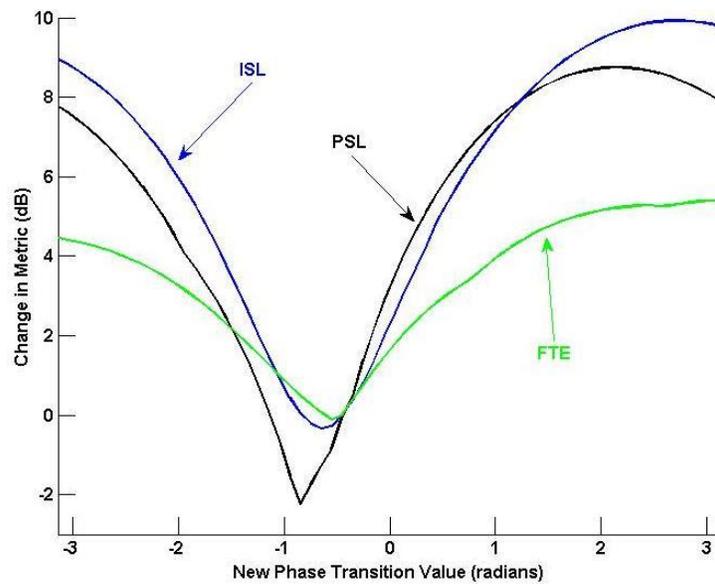

Figure 3: Change in performance metric Φ (for PSL, ISL, and FTE) as a function of different values for phase transition $n = 23$
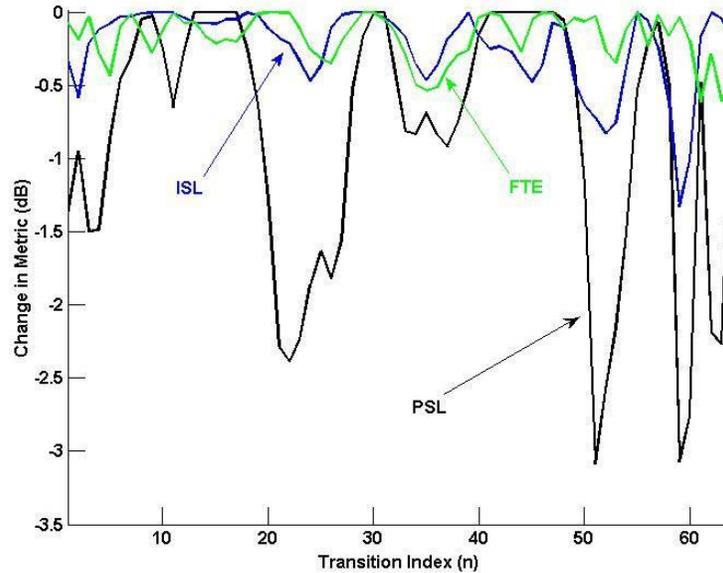
Figure 4: Best change in performance metric Φ (for PSL, ISL, and FTE) as a function of transition index n. The different metrics indicate that different transition indices are the best: PSL($\hat{n} = 51$), ISL($\hat{n} = 59$), and FTE($\hat{n} = 61$)

Employing this performance diversity paradigm, it has been found that emission optimization performance for all these complementary metrics can be significantly improved when a policy is instituted whereby the particular assessment metric is varied for different optimization stages. The nature of the policy is arbitrary and could involve, for example, a fixed interval of permutation stages for each metric in turn or, alternatively, an independent random selection of the metric for each stage. While global optimality is still not guaranteed, this form of metric-varying optimization helps avoid more of the local minima, since convergence would only halt if none of the metrics could provide sufficient further improvement.

IV. DISTORTION-FREE OPTIMIZATION

To evaluate the efficacy of this new design approach in the context of existing waveforms, first consider the case of an idealized transmitter with no distortion. To assess the performance of optimized PCFM waveforms, comparisons are made with the

well-known LFM chirp and the linear period modulation (LPM) waveform (otherwise known as hyperbolic FM, a class of NLFM [8]). For the same time-bandwidth product, these waveforms provide benchmarks for range resolution (LFM) and PSL (LPM). Specifically, because a reduction in range sidelobes corresponds to better spectral roll-off, the result is degradation in range resolution compared to the LFM benchmark. However, the PSL value for LFM is known to be quite high at -13.5 dB. In contrast, LPM waveforms have a lower bound on PSL of [7]

$$\mathrm{PSL}_{\mathrm{LPM\ bound}} = -20\log_{10}(BT) - 3 \ \mathrm{dB} \tag{16}$$

for time-bandwidth product BT, which establishes a useful benchmark for sensitivity.

For the idealized transmitter, no distortion occurs so $u(t;\mathbf{x}) = T_{\mathrm{Tx}}\big[s(t;\mathbf{x})\big] = s(t;\mathbf{x})$. Consider optimizing this idealized PCFM emission for a phase-transition code $\mathbf{x}$ comprised of 64 $(= N)$ elements, where each individual value of α can take on one of 64 $(= L)$ phase transitions drawn from a uniform sampling on the interval $[-\pi, \pi]$ and indexed as $\ell \in 1, 2, \cdots, L$, where $\ell = 1$ corresponds to $\alpha = -\pi$ and $\ell = L$ corresponds to $\alpha = +\pi$. Consequently, we may express the nth phase transition α_n with index ℓ_n as

$$\alpha_n = 2\pi\left(\frac{\ell_n - 1}{L - 1}\right) - \pi \tag{17}$$

for $n = 1, 2, \cdots, N$. Here the CPM implementation employs the rectangular (RECT) shaping filter [13] which, using (17), closely approximates an LFM waveform when $\ell_n = n$. The optimization process is initialized with this LFM coding and the autocorrelation mainlobe for (12) and (14) is defined with $\tau_{\mathrm{m}} = \min[\tau_{\mathrm{null}}, 2.5T_p]$ where

τ_{null} is the distance from the mainlobe peak to the 1$^{\text{st}}$ null and $2.5T_p$ is used to bound the mainlobe width, for T_p the transition interval defined in [13].

According to the mainlobe bandwidth for PCFM waveforms as defined in [13, Sect. 3], it is straightforward to show that N provides an approximate upper limit on the time-bandwidth product (based on the first spectral null). Hence, for $N = 64$ the bound from (16) reveals a PSL lower limit of -39.1 dB for LPM waveforms [7].

Using the metrics for PSL (12), ISL (14), and FTE (15) separately, Fig. 5 shows the autocorrelations of the resulting optimized waveforms. In each case, the search process from (11) is applied until no further convergence is observable (that is, a local minimum is reached). Also shown in Fig. 5 is the result obtained from the performance diversity paradigm in which the search process from (11) is repeated using the metric ordering {ISL, PSL, FTE, ISL, PSL, FTE, ISL, PSL, FTE, PSL}, where the converged local minimum solution for the metric in each step serves as the initialization of the next step. This ordering is arbitrary, with the cycling structure used to avoid a successive repeat of the same metric which would have no benefit. A comparison of the four cases (ISL, PSL, FTE, and performance diversity) reveals that performance diversity yields substantial improvement in sidelobe levels relative to the three individual metrics.
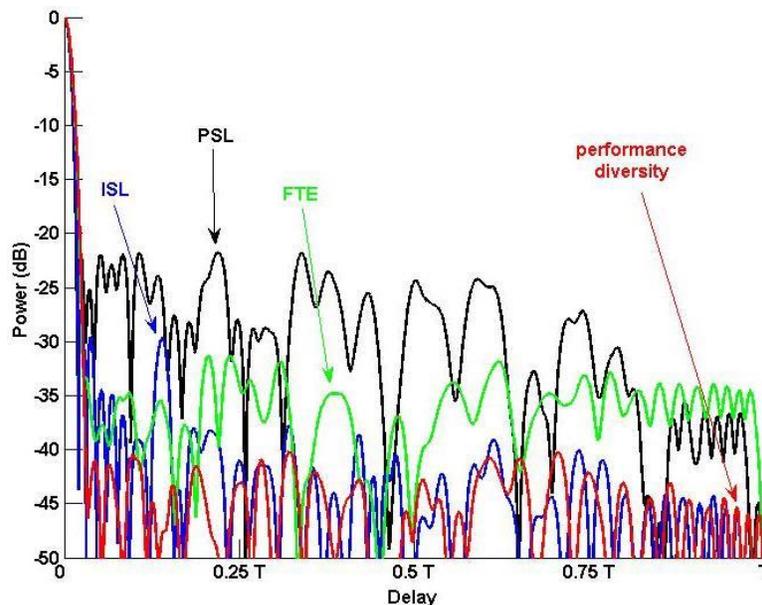
Figure 5: Autocorrelation of the optimized ideal emissions using the PSL, ISL, and FTE metrics individually and the performance diversity paradigm
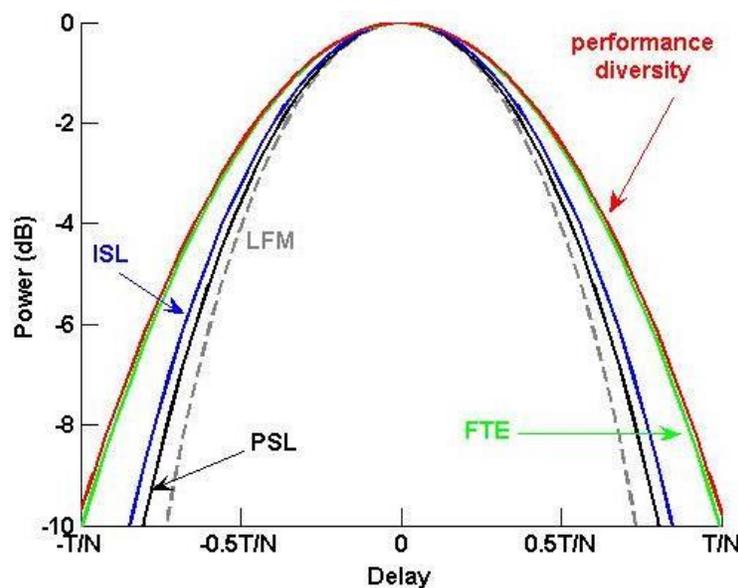

Figure 6: Autocorrelation of the optimized ideal emissions using the PSL, ISL, and FTE metrics individually and the performance diversity paradigm (mainlobe zoom-in)

Figure 6 illustrates the mainlobe width for the different waveforms relative to the LFM waveform. Table 1 quantifies the resolution for 3 dB and 6 dB mainlobe widths relative to that of the baseline LFM waveform and the final PSL, ISL, and FTE metrics for the four optimized waveforms (ISL only, PSL only, FTE only, and performance

diversity). It is found that optimization according to PSL only yields the least improvement over LFM for all three performance metrics (based on final PSL, ISL, and FTE values). That said, PSL optimization experiences little range resolution degradation relative to LFM. While a marked improvement is observed when using ISL or FTE individually, the clear winner in terms of sidelobe reduction is when all three metrics are used in the framework of performance diversity. In fact, the final PSL value of -40.2 dB for performance diversity is 1.1 dB better than the -39.1 dB lower bound defined above for LPM waveforms. The trade-off for such improvement is a ~30% degradation in range resolution (mainlobe broadening) relative to LFM.

Table 1: Quantified performance for optimization of idealized emissions

	LFM waveform	Optimization Metrics			
		PSL only	ISL only	FTE only	Performance Diversity
final PSL value (dB)	−13.5	−21.1	−27.0	−31.3	−40.2
final ISL value (dB)	−9.8	−6.7	−20.0	−15.6	−24.9
final FTE value (dB)	−17.0	−16.6	−22.4	−30.1	−32.1
relative 3 dB resolution	1.00	1.06	1.11	1.26	1.28
relative 6 dB resolution	1.00	1.08	1.13	1.30	1.33

Table 2 provides the indices employed by (17) to generate the resulting optimized PCFM waveforms. It is interesting to consider the associated phase transition sequences shown in Fig. 7 which represent the time-frequency behavior. Compared to the initial linear phase transition sequence using $\ell_n = n$ and $L = N$ in (17) that closely approximates LFM, the four optimized waveforms exhibit a seemingly random dithering that actually serves to break up the coherency which otherwise produces higher sidelobes. This dithering aside, careful examination shows that all four waveforms follow a roughly sideways S-shaped path close to the linear trajectory that is akin to traditional NLFM [3, Sect. 5.2]. Also, the PSL and FTE sequences have short-term wideband components that

are similar to the emissions of some species of bats (see Rhinolophidae and Mormoopidae in [25]).

Table 2: Phase transition indices (vector x) for optimized ideal emissions based on (17)

| ISL only	1,1,1,3,10,6,10,13,14,13,14,15,17,18,19,21,21,22,22,23,23,24,28,26,29,26,30,30,30,33, 27,33,33,37,35,34,36,37,38,39,38,38,42,42,44,44,43,44,46,46,47,49,51,52,51,55,49,57, 58,58,62,64,64,64
PSL only	9,57,3,4,7,8,55,5,11,10,12,14,16,16,61,15,20,21,18,24,18,21,25,21,23,41,26,29,28,28, 28,34,33,37,35,35,39,38,37,41,43,39,44,43,47,39,48,48,48,48,49,53,52,54,53,57,56,60, 61,61,61,64,64,64
FTE only	2,2,7,9,10,14,13,12,19,12,18,19,18,20,21,22,23,22,21,24,25,25,28,25,27,30,29,28,29, 30,30,33,32,34,34,34,35,36,35,37,36,37,41,39,42,43,39,43,42,45,43,48,47,49,49,51,49, 54,53,57,62,64,64,1
Performance Diversity	1,1,3,7,12,14,12,15,16,16,16,19,20,20,22,23,23,23,23,24,25,26,28,28,30,29,28,29,29, 32,32,34,31,33,34,37,36,36,35,37,36,39,39,40,43,40,43,41,42,43,45,45,47,50,47,48,51, 52,51,55,57,61,64,64
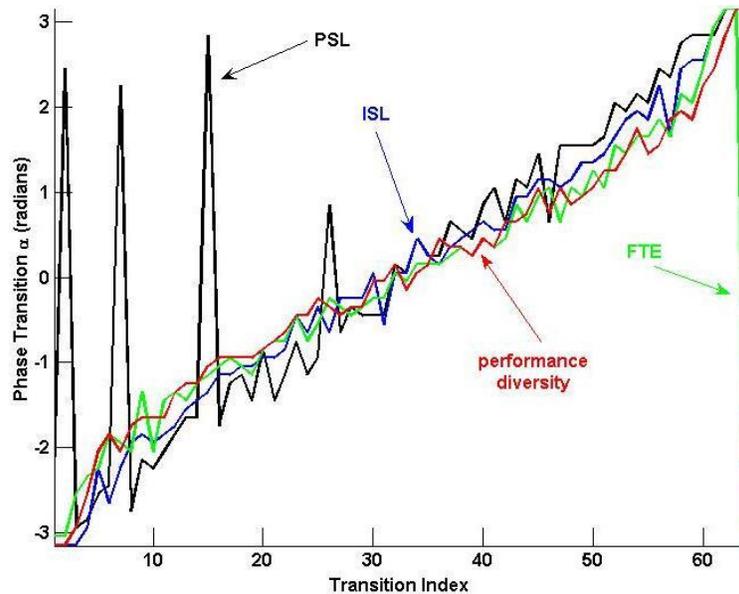
Figure 7: Discrete phase transition sequence x of emissions optimized for PSL, ISL, and FTE individually and using performance diversity.

In terms of unwrapped phase, the PCFM waveforms generated by the four **x** sequences in Table 2 still approximate the parabolic shape associated with the LFM phase progression (Fig. 8). Thus the Doppler tolerance property is also largely retained. A close-up of the delay-Doppler ambiguity function for the performance diversity optimized waveform is shown in Fig. 9. Where traditional NLFM waveforms possess

significant deviation from LFM at the ends of the pulse, which leads to additional ridges near the main range-Doppler ridge, these ridges are rather small for the optimized PCFM waveforms because the deviation from linear now takes the form of localized frequency dithering (Fig. 7). For the performance diversity ambiguity function (Fig. 9), the largest range-Doppler sidelobe value outside the main delay-Doppler ridge is −16.4 dB.
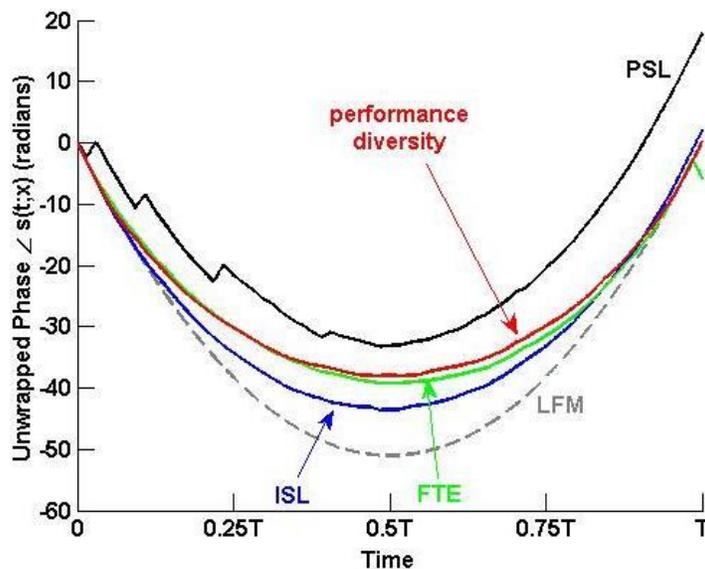

Figure 8: Continuous phase progression of emissions optimized for PSL, ISL, and FTE individually and using performance diversity.   Standard LFM is included for comparison.
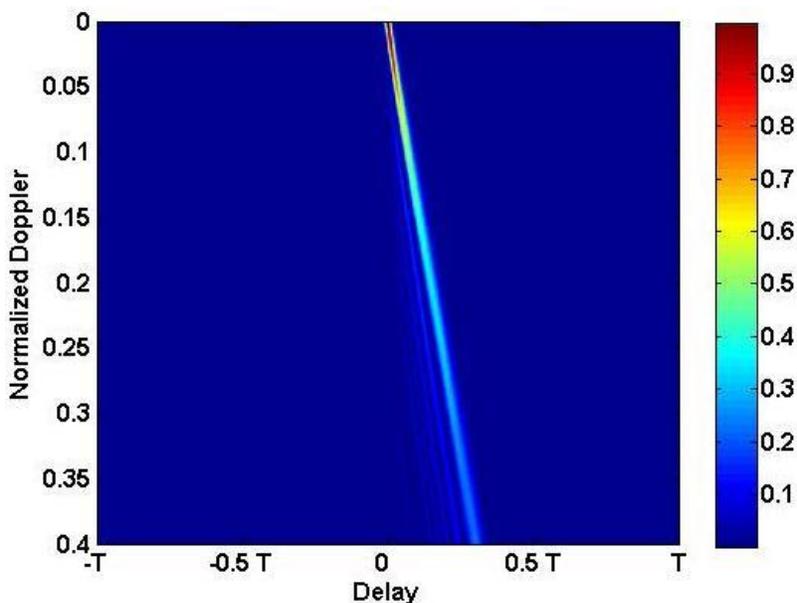

Figure 9: Partial delay-Doppler ambiguity function of the emission optimized under the performance diversity framework

V. OPTIMIZATION OF RADAR EMISSIONS

Now consider the impact of transmitter distortion and the use of transmitter-in-the-loop optimization to compensate for distortion-induced sensitivity degradation. The radar transmitter is comprised of multiple components (mixers, filters, amplifiers, etc.) that contribute to the distortion of the waveform. The most prominent source of distortion tends to be the power amplifier, which induces a nonlinear amplitude compression as a result of being operated in saturation to achieve high power efficiency.

There are essentially two ways in which the transmitter may be incorporated into the process of optimizing the radar emission: 1) a Model-in-the-Loop (MiLo) formulation that employs a mathematical model of the transmitter; and 2) direct use of Hardware-in-the-Loop (HiLo). The former can exploit the benefits of high-performance computing and massive parallelization to search efficiently for an optimized emission. However, the MiLo approach cannot account for all attributes of the transmitter and thus there is a limit to the fidelity that it can provide. In contrast, the HiLo approach allows the emission to be tuned precisely to the physical hardware, though the physical generation of candidate emissions and their subsequent capture for performance evaluation can introduce significant latency into the optimization process. Both approaches are considered in the next two subsections.

A) MiLo Optimization

The simplest approach for transmitter MiLo optimization can be realized using an IIR filter such as a Chebyshev filter followed by a mathematical model of the amplitude compression of the power amplifier. The filter replicates the spectral shaping of the physical system and provides more realistic rise and fall times for the pulse along with

the amplitude ripple and phase distortion of a physical system. The power amplifier causes nonlinear distortion that compounds the filtering effects.

Extensive work exists on modeling power amplifier distortion. In this analysis, the model of a solid-state amplifier from [17] is adopted as it approximates the physical amplifier to be used in the subsequent hardware assessment. Note that greater distortion can be expected for tube-based power amplifiers, which remain in widespread use.

Denoting $\tilde{s}(t;\mathbf{x})$ as the filtered version of the waveform that is input to the power amplifier, the model-based emission can be expressed as

$$u(t;\mathbf{x}) = G\big[\tilde{s}(t;\mathbf{x})\big]\,\tilde{s}(t;\mathbf{x}),\tag{18}$$

where the compression term G is

$$G[r] \triangleq \frac{A(|r|)}{|r|}\tag{19}$$

and

$$A(r) = \frac{v\,r}{\left[1+\left(\dfrac{v\,r}{A_0}\right)^{2b}\right]^{1/2b}}.\tag{20}$$

In (20), v is the small-signal gain, A_0 is the saturating amplitude at the amplifier output, and b is an integer that controls the softness of transition from linear to nonlinear. For the ensuing results the values $v=10$, $A_0 = 1$, and $b=3$ are used.

Figure 10 shows (in blue) the autocorrelation of the performance diversity waveform optimized for an ideal transmitter (from Sect. IV). Driving this waveform into the model above introduces distortion that produces increased sidelobe levels (in red) in the amount of 4.6 dB for the PSL metric and 2.8 dB for the ISL metric (interestingly, the FTE metric

does not change). Applying the performance diversity approach to now optimize the model-distorted emission (black trace) provides 4.4 dB of lost sensitivity for the PSL metric and 2.2 dB for the ISL metric. However, the FTE metric is now degraded by 2.1 dB. Table 3 quantifies the various metrics.
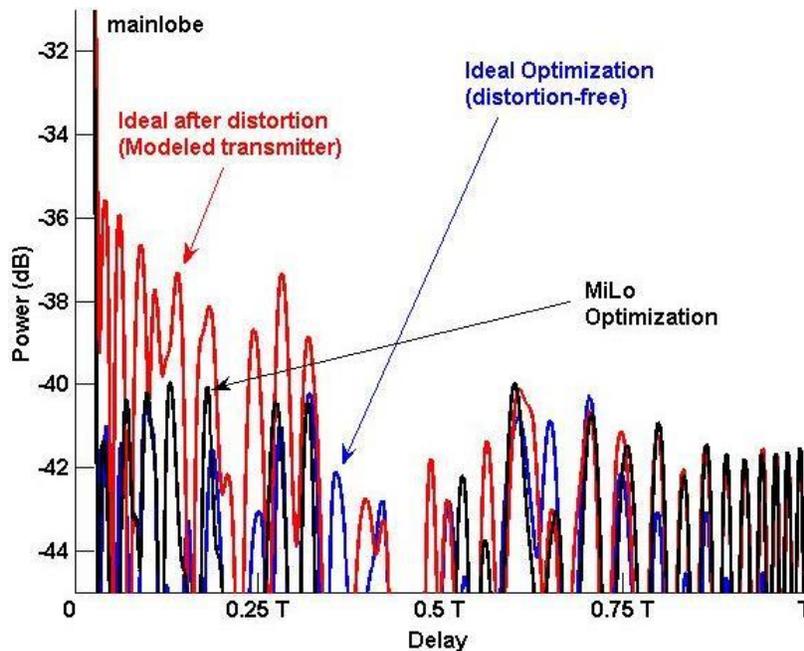

Figure 10: Emission autocorrelation for the ideal optimization (distortion-free) case, the modeled transmitter distortion case, and transmitter Model-in-the-Loop (MiLo) optimization

Table 3: Quantified Performance for MiLo Optimization

	Ideal Optimization	After Tx Model	MiLo Optimization
final PSL value (dB)	−40.2	−35.6	−40.0
final ISL value (dB)	−24.9	−22.1	−24.3
final FTE value (dB)	−32.1	−32.1	−30.0
relative 3 dB resolution	1.28	1.23	1.23
relative 6 dB resolution	1.33	1.28	1.27

B) HiLo Optimization

Direct incorporation of the physical transmitter into the optimization process naturally accounts for the eccentricities of the hardware and thus can be expected to provide the most accurate result. To demonstrate the efficacy of HiLo optimization, the

L-band (f_c = 1.842 GHz) radar test bed depicted in Fig. 11 is used with the anechoic chamber at the University of Kansas to perform free-space emission optimization that includes antenna effects. Here a Class A power amplifier is used which, in an attempt to mimic some of the distortion effects of a high-power amplifier, is driven well into saturation. Specifically, the 1 dB compression point for the amplifier is 6 dBm, and the input power driving the amplifier is 11 dBm (thus 5 dB into saturation).

Following the CPM implementation of a candidate code (performed digitally in Matlab), the resulting PCFM waveform is converted to in-phase and quadrature-phase (I/Q) components and is then loaded onto the arbitrary waveform generator (AWG). The AWG drives the waveform into a single sideband (SSB) modulator that upconverts the waveform to L-band. The upconverted waveform is passed through the saturated solid-state power amplifier and a quad-ridge horn transmit antenna. The receive antenna is a standard-gain horn. Following attenuation and downconversion in the receiver, the subsequent baseband signal is sampled by the digitizer and passed back to a Matlab program running on a laptop (Fig. 11), where the emission is assessed. Due to the absence of receiver clipping it is assumed that any distortion induced within the receive chain is negligible relative to that introduced by the transmitter.

The performance diversity emission, optimized under ideal conditions from Section IV, is again used as the initialization. Due to buffering delays in the arbitrary waveform generator and the digitizer, the HiLo operation on this test bed is much slower than what could be achieved in the MiLo case in simulation. Thus, only the PSL metric from (12) is used to drive emission optimization. In practice, a high-fidelity model of the system

could be employed to obtain an initialization via MiLo that should subsequently only require fine tuning with HiLo optimization.

As expected, the transmitter hardware distorts the idealized emission (Fig. 12) yielding 2.7 dB of PSL degradation. HiLo optimization is able to recover 1.5 dB of this lost sensitivity. Table 4 quantifies the results according to the various metrics. Due to the use of an available Class A power amplifier, the degree of degradation was rather limited. Further studies are planned to investigate the amount of degradation and subsequent performance recovery that can be obtained for high-power tube-based amplifiers.

Figure 11: L-band radar test bed (anechoic chamber in background)

Table 4: Quantified performance for HiLo Optimization

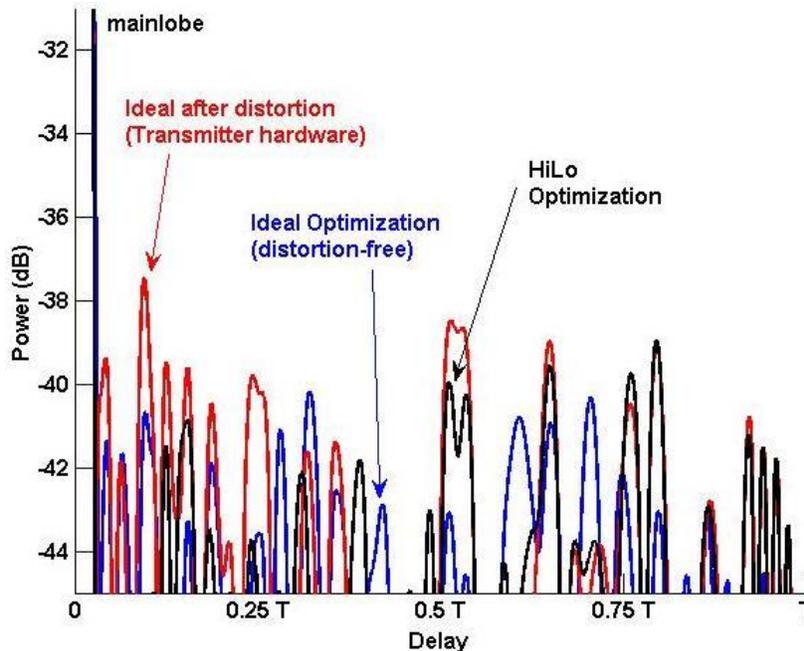|	Ideal Optimization	After Tx Hardware	HiLo Optimization
final PSL value (dB)	−40.2	−37.5	−39.0
final ISL value (dB)	−24.9	−23.4	−24.6
final FTE value (dB)	−32.1	−30.5	−30.9
relative 3 dB resolution	1.28	1.25	1.25
relative 6 dB resolution	1.33	1.23	1.23

Figure 12: Emission autocorrelation for the ideal optimization (distortion-free) case, the physical (hardware) transmitter distortion case, and transmitter Hardware-in-the-Loop (HiLo) free-space optimization

CONCLUSIONS

In this second paper of a two-part sequence, it was shown that the continuous phase modulation (CPM) implementation of polyphase-code FM (PCFM) waveforms provides a linkage that connects the code to the continuous waveform and ultimately to the physical radar emission. As a result, the degrees of freedom of the code become the means with which to optimize the radar emission while naturally incorporating the intrinsic spectral shaping and nonlinear distortion of the transmitter. For the case of an idealistic transmitter (no distortion), it was shown that an optimized PCFM waveform can be obtained that exceeds the PSL benchmark established for linear period modulation (LPM) waveforms without the need for amplitude weighting of the pulse. When using either a mathematical model for the transmitter distortion or physical transmit hardware, the Model-in-the-Loop (MiLo) and Hardware-in-the-Loop (HiLo) optimization schemes

demonstrated the capability to recapture the lost sensitivity due to transmitter distortion. This work sets the stage for the physical optimization of high-power radar emissions, the design of emissions for exotic transmitter topologies proposed to enable better spectral containment, and numerous new waveform diversity approaches.

REFERENCES

[1] J. Jakabosky, P. Anglin, M.R. Cook, S.D. Blunt, and J. Stiles, "Non-linear FM waveform design using marginal Fisher's information within the CPM framework," *IEEE Radar Conf.,* pp. 513-518, Kansas City, MO, May 2011.

[2] J. Jakabosky, S.D. Blunt, M.R. Cook, J. Stiles, and S.A. Seguin, "Transmitter-in-the-loop optimization of physical radar emissions," *IEEE Radar Conf.,* pp. 874-879, Atlanta, GA, May 2012.

[3] N. Levanon and E. Mozeson, *Radar Signals*, John Wiley & Sons, Inc., Hoboken, NJ, 2004.

[4] E. Fowle, "The design of FM pulse compression signals," *IEEE Trans. Information Theory*, vol. 10, no. 1, pp. 61-67, Jan. 1964.

[5] C.E. Cook, "A class of nonlinear FM pulse compression signals," *Proceedings of the IEEE*, vol. 52, no. 11, pp. 1369-1371, Nov. 1964.

[6] R. De Buda, "Stationary phase approximations of FM spectra," *IEEE Trans. Information Theory*, vol. 12, no. 3, pp. 305-311, July 1966.

[7] T. Collins and P. Atkins, "Nonlinear frequency modulation chirps for active sonar," *IEE Proc. Radar, Sonar & Navigation*, vol. 146, no. 6, pp. 312-316, Dec. 1999.

[8] J.J. Kroszczynski, "Pulse compression by means of linear-period modulation," *Proc. IEEE*, vol. 57, no. 7, pp. 1260-1266, July 1969.

[9] A.W. Doerry, "Generating nonlinear FM chirp waveforms for radar," *Sandia Report*, SAND2006-5856, Sept. 2006.

[10] I. Gladkova, "Design of frequency modulated waveforms via the Zak transform," *IEEE Trans. Aerospace & Electronic Systems*, vol. 40, no. 1, pp. 355-359, Jan. 2004.

[11] J.A. Johnston and A.C. Fairhead, "Waveform design and Doppler sensitivity analysis for nonlinear FM chirp pulses," *IEE Proc. F – Communications, Radar & Signal Processing*, vol. 133, no. 2, pp. 163-175, Apr. 1986.

[12] E. De Witte and H.D. Griffiths, "Improved ultra-low range sidelobe pulse compression waveform design," *Electronics Letters*, vol. 40, no. 22, pp. 1448-1450, Oct. 2004.

[13] S.D. Blunt, M. Cook, J. Jakabosky, J. de Graaf, E. Perrins, "Polyphase-coded FM (PCFM) waveforms, part I: implementation," to appear in *IEEE Trans. AES*.

[14] C.J. Nunn and G.E. Coxson, "Polyphase pulse compression codes with optimal peak and integrated sidelobes," *IEEE Trans. Aerospace & Electronic Systems*, vol. 45, no. 2, pp. 775-781, Apr. 2009.

[15] A. Nehorai, F. Gini, M.S. Greco, A.P. Suppappola, and M. Rangaswamy, Special Issue on "Adaptive waveform design for agile sensing and communication," *IEEE Journal of Selected Topics in Signal Processing*, vol. 1, no. 1, June 2007.

[16] J.D. Jenshak and J.M. Stiles, "A fast method for designing optimal transmit codes for radar," *IEEE Radar Conf.*, Rome, Italy, May 2008.

[17] E. Costa, M. Midrio, S. Pupolin, "Impact of amplifier nonlinearities on OFDM transmission system performance," *IEEE Communications Letters*, vol. 3, no. 2, pp. 37-39, Feb. 1999.

[18] F.H. Raab, P. Asbeck, S. Cripps, P.B. Kenington, Z.B. Popovic, N. Pothecary, J.F. Sevic, and N.O. Sokal, "Power amplifiers and transmitters for RF and microwave," *IEEE Trans. Microwave Theory & Techniques*, vol. 50, no. 3, Mar. 2002, pp. 814-826.

[19] C. Balanis, *Antenna Theory*, Wiley-Interscience, 2005, Sect. 8.7.

[20] S.D. Blunt, T. Chan, and K. Gerlach, "Robust DOA estimation: the reiterative superresolution (RISR) algorithm," *IEEE Trans. Aerospace & Electronic Systems*, vol. 47, no. 1, pp. 332-346, Jan. 2011.

[21] B. Cordill, J. Metcalf, S.A. Seguin, D. Chatterjee, and S.D. Blunt, "The impace of mutual coupling on MIMO radar emissions," *IEEE Intl. Conf. on Electromagnetics in Advanced Applications*, pp. 644-647, Torino, Italy, Sept. 2011.

[22] J. Li and P. Stoica, *MIMO Radar Signal Processing*, John Wiley & Sons, Inc., Hoboken, NJ, 2009.

[23] D.A. Pierre, *Optimization Theory with Applications*, Dover Publications, 1986.

[24] M.A. Richards, J.A. Scheer, and W.A. Holm, *Principle of Modern Radar: Basic Principles*, SciTech Publishing, 2010, pp. 793-794.

[25] M. Vespe, G. Jones, and C.J. Baker, "Lesson for radar: waveform diversity in echolocating mammals," *IEEE Signal Processing Magazine*, vol. 26, no. 1, pp. 65-75, Jan. 2009.